Radiation-driven Destruction of Thiophene and Methyl-Substituted Thiophenes

Patrick D. Tribbett,[1,2,3] Yukiko Y. Yarnall,[1,2,3] Reggie L. Hudson,[2] Perry A. Gerakines,[2] Christopher K. Materese[2]

[1] Center for Space Science and Technology, University of Maryland Baltimore County, Baltimore, MD 21250, USA

[2] Astrochemistry Laboratory, NASA Goddard Space Flight Center, Greenbelt, MD 20771, USA

[3] Center for Research and Exploration in Space Science and Technology, NASA Goddard Space Flight Center, Greenbelt, MD 20771, USA

Abstract:

Thiophene and two derivatives (2-methylthiophene and 3-methylthiophene) have been detected on the surface of Mars with the Sample Analysis at Mars (SAM) instrument suite onboard NASA's Curiosity rover. Thiophene could serve as a secondary chemical biosignature since the secondary biosynthesis of thiophene is considered an important production pathway. However, it is critical to understand the abiotic formation and destruction of thiophene and its derivatives since these pathways could affect the molecules' stabilities on planetary surfaces over geological timescales. Here, we present the radiolytic destruction kinetics of thiophene, 2-methylthiophene, and 3-methylthiophene as single-component ices and when diluted in water ice at low temperatures. Using infrared spectroscopy, we determined the destruction rate constants and

extrapolated our radiolytic half-lives to the surface of Mars, assuming the measured and modeled surface dose rates. We found that our rate constants strongly depend on temperature and presence of water ice. Based on our determined radiolytic half-life for thiophene under conditions most similar to those of thiophene groups in Martian macromolecules, we expect thiophene to be stable on the surface for significantly longer than the Martian surface exposure age of sites in Gale crater where thiophenes have been detected.

1. Introduction:

The Martian surface and subsurface contain organic molecules trapped in macromolecular structures embedded in clay-bearing sediments. These organic molecules, in addition to the geological features that suggest the presence of surface and subsurface liquid water, provide mounting evidence of a potentially habitable environment in Mars' distant past. The identities and chemical pathways (*e.g.*, production and destruction) of these organic molecules directly probe the astrobiological potential of ancient, wet Mars.

Instruments onboard the Mars Science Laboratory's Curiosity rover identified a variety of organic molecules at various sites in Gale crater, a location selected for its evidence of ancient aqueous activity and potential for astrobiology (Wray, 2013; Vasavada, 2022). Data from the pyrolysis evolved gas analysis (EGA) and gas chromatography-mass spectrometry (GC-MS) instrument suite onboard Curiosity rover revealed the presence of likely indigenous chlorobenzene (Freissinet et al., 2015), which is consistent with a reanalysis of data from the Viking landers (Guzman et al., 2018). More recent efforts using the pyrolysis EGA and GC-MS instruments detected several sulfur-bearing organic molecules, including thiophene and

alkylthiophenes (2-methylthiophene and 3-methylthiophene) in samples from lacustrine mudstones in Gale crater (Eigenbrode et al., 2018; Millan et al., 2022).

The structures for thiophene (C_4H_4S), 2-methylthiophene (C_5H_6S), and 3-methylthiophene (C_5H_6S) are shown in Figure 1. Both thiophene and alkylthiophenes are likely indigenous to the Martian surface as components of refractory organic macromolecules, which was inferred from the pyrolysis temperatures required for decomposition of the macromolecules and subsequent thiophene detection. Interestingly, these previous studies suggested that thiophene and alkylthiophenes could serve as preserved secondary chemical biosignatures on Mars due to their importance in the preservation of organic material on Earth. Terrestrially, thiophenes form through reactions between reduced sulfur (*e.g.*, H_2S) and various organic materials during the diagenesis of sedimentary material, and both of these "reactants" can be biotic or abiotic in origin (see report by Heinz and Schulze-Makuch, 2020, and references therein). Li et al. (2023) demonstrated that collisions between gas-phase sulfur atoms and conjugated dienes, including 1,3-butadiene and isoprene, might provide additional abiotic pathways to form thiophenes, and these pathways may be important for planetary and interstellar environments.

Unlike Earth, Mars lacks a global magnetic field capable of shielding its surface from radiation, which allows galactic cosmic rays (GCRs) and solar energetic particles (SEPs) to penetrate through the thin CO_2 atmosphere (Acuña et al., 1998). Given enough incident energy, these particles penetrate into the regolith, depositing energy in the surface and creating secondary energetic particles that induce chemistry. GCRs provide the dominant source of radiation to the top three meters of the Martian regolith (Hassler et al., 2014). This radiation-driven chemistry decomposes or degrades organic molecules, providing a destruction pathway for molecules that

serve as potential biosignatures. Previous laboratory work has demonstrated that biologically important molecules, including amino acids (Gerakines et al., 2012; Gerakines and Hudson, 2013, 2015; da Costa et al., 2021; Mejía et al., 2022) and nucleobases (Materese et al., 2020; Gerakines et al., 2022; Vignoli Muniz et al., 2022; Mejía et al., 2023), decompose when exposed to ionizing radiation (Tolbert and Lemmon, 1955). Thus, to effectively use thiophene or a thiophene derivative as a secondary biosignature, it is critical to understand the effects of radiation on thiophene groups within larger solid macromolecules. Early works examined the effects of radiation on liquid thiophene or aqueous solutions of thiophene and identified many of the radical intermediate species produced (Saunders et al., 1978; Saunders, 1978). However, the rate of radiation-driven destruction of thiophene or of its derivatives in the solid phase, as would be expected on Mars, remains undetermined. These rates provide additional astrochemical context to the recent detections of thiophene and alkylthiophenes on the surface of Mars.

Here, we report the results of laboratory experiments to measure the radiation-induced destruction of thiophene and thiophene derivatives as single-component ices and when mixed with water ice at 20 and 125 K. We identify the likely radiolytic products and quantify the rates of destruction with infrared (IR) spectroscopy. Lastly, we describe the implications of our destruction rates for the Martian surface.

2. Experimental Methods:

We performed all experiments in a high-vacuum chamber with a base pressure of $\sim 1 \times 10^{-7}$ Torr at the lowest temperature studied (Hudson and Ferrante, 2020; Qasim et al., 2022; Materese, 2022). Briefly, we vapor-deposited samples onto a pre-cooled KBr or ZnSe substrate in thermal contact with a helium cryostat. Note that the choice of substrate did not alter the acquired

spectra. We produced single-component ices or ice mixtures at 20 and 125 K. While these temperatures are considerably lower than the average Martian surface temperature (~ 220 K near the equatorial latitudes; Vasavada et al., 2017), thiophene and its derivatives begin to substantially sublimate above 125 K in our vacuum chamber, which limits our experimental temperature. All compounds were degassed by three freeze-pump-thaw cycles with liquid nitrogen to remove excess dissolved gases from the samples prior to vapor deposition. We determined the ice thickness by using the interference fringes of a 670 nm laser near perpendicular to the substrate. For mixtures, we co-deposited each compound from independent vapor lines using pre-calibrated leak valves to achieve a relative ratio of water to thiophene or thiophene derivative of 100:1 (i.e., 100 water molecules for every 1 thiophene or thiophene derivative molecule). This mixture ratio was chosen to isolate the thiophene or thiophene derivative molecules within the matrix and limit interactions between organic molecules during radiolysis while maintaining sufficient IR signal-to-noise to quantify the radiolytic destruction.

We determined the deposition rate of the organic molecules required to produce the desired relative ice composition using

$$\frac{\text{water deposition rate}}{\text{thiophene deposition rate}} = \frac{100}{1} \times \frac{\rho_{\text{thiophene}}}{\rho_{\text{water}}} \times \frac{M_{\text{water}}}{M_{\text{thiophene}}} \times \frac{n_{\text{water}}}{n_{\text{thiophene}}} \quad (1)$$

where ρ is the density (g cm^{-3}), M is the molar mass (g mol^{-1}), and n is the index of refraction at 670 nm. We observed 4 and 8 interference fringes for our single-component ices and ice mixtures respectively, and determined the total ice thickness using equation 2 (given in Heavens, 2011)

$$h = \frac{N_{\text{fringes}}\lambda}{2\sqrt{n^2 - \sin^2\theta}} \quad (2)$$

where N_{fringes} is the number of fringes, λ is the wavelength of the laser (670 nm), and θ is the angle of incidence for the interference laser. We calculated the column density from equation 3

$$N = \frac{h\,\rho_{\text{water}}\,N_A}{M_{\text{water}}} \quad (3)$$

where h is the total thickness of the ice, and N_A is Avogadro's constant. The thicknesses of our ice samples ranged between 0.9 and 2 μm. We determined the densities and refractive indices for thiophene, 2-methylthiophene, and 3-methylthiophene at 18 K following the standard procedures used in the Cosmic Ice Laboratory (Yarnall and Hudson, 2022a, b). These values are the first measurements of the density and index of refraction for thiophene and thiophene derivatives as ices (see Table 1). Interestingly, the relative ordering for the densities of thiophene and its derivatives is consistent with measurements of their liquid densities (i.e., thiophene > 3-methylthiophene > 2-methylthiophene) (Weast et al., 1984).

After deposition, we irradiated the ice with ~ 0.9 MeV protons generated by a Van de Graff accelerator and directed perpendicular to the substrate surface (Loeffler and Hudson, 2018) at a current of 0.5×10^{-7} A or an ion flux of 2.53 x 10^{11} proton cm^{-2} s^{-1}. We calculated the dose absorbed by the ice in units of MGy according to

$$\text{Dose} = \text{S} \times \text{F} \times (1.602 \times 10^{-22}) \quad (4)$$

where F is the fluence (in units of protons cm^{-2}) determined from the total integrated current, S is the total proton stopping power in each ice (in units of eV cm^2 g^{-1} $proton^{-1}$), and a multiplicative factor converts the dose from eV g^{-1} to MGy. Both the 0.9 MeV protons used in this study and the GCRs impacting the surface of Mars produce low-energy (~ 10 eV) secondary electrons that facilitate much of the observed chemistry (Pimblott and LaVerne, 2007). For additional discussion regarding the application of laboratory radiolysis studies to the Martian surface see the work of Gerakines and Hudson (2015), and references therein. We calculated the total proton stopping power in each ice using the Stopping and Range of Ions in Matter (SRIM) software (Ziegler et al, 2010), and those values can be found in Table 1. Ices were irradiated to an

138 absorbed dose of ~ 75 MGy and ~ 19 MGy, for single-component ices and water-ice mixtures
139 respectively. These doses correspond to approximately ~ 1 billion years and ~ 250 million years
140 on the surface of Mars (assuming a dose rate of 76 mGy yr^{-1}; Hassler et al., 2014). We quantified
141 the radiation-driven destruction of thiophene and its derivatives *in situ* using transmission IR
142 spectroscopy. We acquired spectra before and after proton irradiation using a Thermo Nicolet
143 iS50 Fourier transform infrared spectrometer and DTGS detector (5500 – 500 cm^{-1} spectral
144 range, 200 averaged scans, and 4 cm^{-1} spectral resolution).
145
146 **3. Results:**
147 **3.1 Radiolysis of Thiophene and Methyl-Substituted Thiophenes:**
148 Figure 2 contains the IR spectrum of a thiophene ice grown at 125 K and the spectrum after
149 each irradiation step. The initial spectrum is consistent with previous low-temperature (130 and
150 12 K) spectra of solid thiophene (Quigley et al., 1996; Cesaro et al., 1999). Spectral assignments
151 and drawings of the fundamental vibrational modes for thiophene can be found in the works of
152 Rico et al (1965) and Christensen et al. (1988), respectively. Note that the initial thiophene
153 features decrease as the radiation dose increases, which indicates the radiation-driven destruction
154 of thiophene. Additionally, we note the emergence of several absorption features as the
155 thiophene was irradiated. Specifically, distinct features appear at 3267, 3225, and 1514 cm^{-1}, as
156 well as a shoulder at 3067 cm^{-1} (Figure 2). The features at 3067 and 1514 cm^{-1} are consistent
157 with the formation of various bithiophenes, including 2,2'-bithiophene, 3,3'-bithiophene, 2,3'-
158 bithiophene, and a-thienothiophene, and polybithiophenes (Wynberg and Bantjes, 1959; Rasch
159 and Vielstich, 1994); however, we cannot identify the specific isomer(s) produced. The 3067
160 cm^{-1} feature may, in part, also be due to the destruction of the thiophene crystalline lattice at 125

K. The broader features centered at 3267 and 3225 cm^{-1} suggest the formation of alkyne groups (H-C≡C-R). This assignment is consistent with several studies that examined the radiation- and photochemistry of benzene, which is structurally comparable to thiophene since both are fully conjugated planar aromatic molecules. Strazzulla and Baratta (1991) noted the emergence of spectral features at 3288 and 3232 cm^{-1} in irradiated benzene ices and attributed these bands to monosubstituted acetylenes and acetylene, respectively. Ruiterkamp et al. (2005) confirmed these spectral features in irradiated benzene ices and noted that the 3278 cm^{-1} feature might be due to acetylene aggregates. Qi et al. (1999) exposed collimated molecular beams containing thiophene to a 193 ArF excimer laser and identified several photodissociation pathways that included the formation of thioketene and ethyne. More recently, Kim et al. (2006) examined photolyzed 2,5-diiodothiophene using matrix-isolation spectroscopy and found evidence of ethynylthioketene, a ring-opening product of thiophene that contains an alkyne group. The presence of this pair of alkyne-group features in our irradiated thiophene ices suggests that the thiophene ring might open during radiolysis. Radiation product spectral features at ~ 3270, ~ 3230, and ~ 1515 cm^{-1} are present for irradiated thiophene and methyl-substituted thiophene samples at both temperatures studied.

In addition to the radiolytic products mentioned above, we found evidence for radiation-driven amorphization of our ices at 125 K. Previous laboratory and computational studies have demonstrated that liquid thiophene undergoes many stable and metastable crystalline phase transitions between 25 and 125 K when cooled from room temperature (Miyazaki et al., 2021, and references therein), and differentiation between phases with infrared spectroscopy requires higher spectral resolution than 4 cm^{-1} (Migliorini et al., 1974). Regardless of the identity of the specific crystalline structure, our 125 K samples are crystalline. We expect that our vapor-

184 deposited thiophene and methyl-substituted thiophene samples at 20 K are amorphous, based on
185 observations of ices composed of other aromatic heterocycles (e.g., pyridine; Hudson and
186 Yarnall, 2022).
187 Figure 3 contains the spectrum of 2-methylthiophene deposited at 125 K (crystalline) before
188 and after irradiation (to a dose of 37 MGy), and the spectra of amorphous unirradiated 2-
189 methylthiophene and 3-methylthiophene deposited at 20 K for comparison. Although most
190 spectral features decrease after a dose of 37 MGy, several features appear (1077, 1044, and 1035
191 cm^{-1}) or increase (1451 and 1440 cm^{-1}) with dose. These changes are consistent with the
192 appearance of amorphous 2-methylthiophene (Figure 3; 3rd from the top) and suggest that our
193 high-temperature ices undergo partial amorphization, which is likely incomplete as evident from
194 the residual sharpness of the 3098 and 3083 cm^{-1} bands. We note that these spectral changes are
195 greatest near a dose of 37 MGy and gradually decrease up to 75 MGy (data not shown).
196 Additionally, these changes did not occur in our ices that were deposited and irradiated at 20 K.
197 Figure 4 contains the spectrum of 3-methylthiophene deposited at 125 K (crystalline) before
198 and after irradiation (37 MGy), and the spectra of amorphous unirradiated 3-methylthiophene
199 and 2-methylthiophene deposited at 20 K for comparison. Similar to that described above, the
200 spectrum of 3-methylthiophene deposited at 125 K and irradiated to 37 MGy (2nd from the top;
201 Figure 4) resembles the spectrum of 3-methylthiophene deposited at 20 K (3rd from the top;
202 Figure 4), which suggests that the sample undergoes radiation-driven amorphization. This
203 process is likely incomplete based on the shape of the 1451 cm^{-1} band and residual structure near
204 ~ 1030 cm^{-1}.
205 In both Figures 3 and 4, we note that several of the changes might in part be due to radiolytic
206 rearrangement, specifically the migration of the methyl group between the 2nd and 3rd carbon on

207 the thiophene ring (Figure 1). Early studies of aqueous samples containing alkylthiophenes
208 demonstrated the photoisomerization of 2-methylthiophene to 3-methylthiophene (Kellogg et al.,
209 1970). Photoisomerization is also seen for the oxygen-bearing analog alkylfuran in the gas phase
210 (Hiraoka and Srinivasan, 1968). However, for our ices, this isomerization does not seem to be
211 significant since the contribution of the strongest bands of amorphous 2-methylthiophene (1239
212 cm^{-1}) and 3-methylthiophene (1451 cm^{-1}) in the corresponding irradiated crystalline spectra is
213 minimal (Figures 3 and 4).
214 Importantly, the amorphization of our 125 K ices impacts the determination of the radiation-
215 driven destruction rate constants since the band strengths of amorphous materials are typically
216 different for the same bands of crystalline material. To estimate the impact of any radiation-
217 induced amorphization, we grew thiophene or methyl-substituted thiophene ices at 20 K, warmed
218 them to 125 K at a rate of 2 K min^{-1}, and found that the band of interest (~ 1250 cm^{-1} for
219 thiophene and 2-methylthiophene; ~ 1150 cm^{-1} for 3-methylthiophene) increased in area by ~ 15
220 % for thiophene and 3-methylthiophene, and ~ 35% for 2-methylthiophene when the ice
221 crystallized. This increase in band area suggests that we might be overestimating the amount of
222 radiolytic destruction for a fraction of material at 125 K that undergoes radiation-induced
223 amorphization (discussed further in Section 4.1).
224
225 **3.2 Radiolysis of Thiophene in Water:**
226 Figure 5 contains the infrared spectrum of thiophene diluted in a water-ice matrix at a ratio of
227 100:1 grown at 125 K and irradiated with 0.9 MeV p^+. Broad absorption features near 1600 and
228 2200 cm^{-1} dominate the spectrum and correspond to the H_2O bending mode and the second
229 overtone of the lattice vibration, respectively (Hardin and Harvey, 1973; Hagen et al., 1981).

Two much sharper features at 1407 and 1250 cm^{-1} indicate the presence of thiophene in the ice mixture. These features decrease as the radiation dose increases, which indicates radiation-driven destruction of the thiophene. At high doses, we note the emergence of a band at 2340 cm^{-1}, which we attribute to the formation of CO_2. This is consistent with previous laboratory studies that demonstrated that the irradiation of mixtures of H_2O and various hydrocarbons (including CH_4 and C_2H_2) produces CO_2 (e.g., Moore and Hudson, 1998; Palumbo et al., 1998), and similar hydrocarbons (H-C≡C-R) are expected when thiophene or its derivatives are irradiated as described in Section 3.1. In addition to CO_2, a weak band at 2853 cm^{-1} appears, which indicates a small amount of H_2O_2. Also, our ice contained a small D_2O/HOD contamination, evident from the absorption band at 2422 cm^{-1} (Hornig et al., 1958); however, D_2O/HOD does not influence the observed radiation chemistry.

While each of the thiophene-derivative mixtures produces similar radiolytic products, there were several differences when the initial ice mixture was deposited and irradiated at 20 K. Figure 6 contains the infrared spectrum of thiophene diluted in a water-ice matrix at a ratio of 100:1 as deposited at 20 K and after irradiation. In addition to CO_2, which is also produced at 125 K, a spectral feature appears at 2137 cm^{-1}, which we attribute to CO, a known radiolytic and photoproduct of CO_2 (e.g., Moll et al., 1966; Moore et al., 1991). Any CO formed in the ices at 125 K would be expected to sublimate from the ice. The greater abundance of H_2O_2 observed in low-temperature H_2O ices is consistent with the generally accepted formation mechanism of H_2O_2 (i.e., the limited diffusivity of OH radicals below 80 K).

3.3 Radiation Destruction Kinetics:

To quantify the destruction kinetics of thiophene and its derivatives, we assume that the radiation-driven destruction follows reversible pseudo first-order kinetics where

$$\text{Thiophene} \underset{k_2}{\overset{k_1}{\rightleftharpoons}} \text{Products} \tag{5}$$

While this is undoubtedly a simplification, first-order kinetics provide reasonable fits to the data, despite the partial amorphization described in Section 3.1. Our group has successfully applied this analysis technique to ices that contain amino acids (Gerakines et al., 2012; Gerakines and Hudson, 2013, 2015) and nucleobases (Materese et al., 2020; Gerakines et al., 2022). Given the forward and reverse reactions, the differential rate law for the destruction of thiophene or thiophene derivative is written as

$$-\frac{d[\text{Thio}]}{dt} = k_1[\text{Thio}] - k_2[\text{Products}] \tag{6}$$

where k_1 and k_2 are the forward and reverse reaction rate constants. Following Espenson (1981), we solve Equation 6 to give

$$\ln\frac{[\text{Thio}]_t - [\text{Thio}]_\infty}{[\text{Thio}]_0 - [\text{Thio}]_\infty} = -(k_1 + k_2)t \tag{7}$$

where $[\text{Thio}]_\infty$ is the concentration of thiophene or thiophene derivative at equilibrium, $[\text{Thio}]_0$ is the initial concentration of thiophene or thiophene derivative, and $[\text{Thio}]_t$ is the concentration of thiophene or thiophene derivative at some given time *t*. We use the dose, which is proportional to the time-integrated flux (or fluence) that our ice samples receive, as a proxy for time. Moreover, we use the area of the ~ 1250 cm^{-1} fundamental thiophene absorption band as a proxy for the concentration of thiophene or 2-methylthiophene. In the case of our 3-methylthiophene sample, we integrated the 1155 cm^{-1} fundamental absorption feature since the ~ 1239 cm^{-1} appears to increase with radiation dose due to the partial amorphization of the crystalline ice (Section 3.1). These effects are negligible for water-ice mixtures, where all

starting material is amorphous and the radiolytic destruction is dominated by the neutral radicals and ionized products from the water matrix. Additionally, we note that both the 1239 and 1155 cm^{-1} infrared absorption features result from motions made by the thiophene derivative ring (Pennington et al., 1956). Following these considerations, we rewrite equation 7 as

$$\frac{A}{A_0} = \left(1 - \frac{A_\infty}{A_0}\right) e^{-(k_1+k_2)D} + \frac{A_\infty}{A_0} \quad (8)$$

where D is the radiation dose absorbed by the sample (in units of MGy). Equation 8 is functionally equivalent to $y = ae^{-bx} + c$, where a, b, and c are fitted parameters related to the rate constants and equilibrium abundances of thiophene or thiophene derivatives.

We fit this function to our normalized band areas (A/A_0) as a function of dose for each composition at each temperature for the single-component ices and ice mixtures (Figures 7-9) using a least-squares regression, and our best-fit parameters are listed in Table 2. The differences between all respective models and data sets are less than 15% and typically between 0.1 and 4%. Given that $b = k_1 + k_2$, and $a = \left(1 - \frac{A_\infty}{A_0}\right) = \frac{k_1}{k_1+k_2}$, we determined the destruction rate constant from the product $k_1 = ab$, in units of MGy^{-1}. These rate constants are shown in Table 3. In addition to the reaction rate constants, we determined the radiolytic half-life dose for thiophene or thiophene derivative (i.e., the dose required to destroy half of the initial thiophene or thiophene-derivative molecules) from the fitted parameters, where $D_{1/2} = -\ln\left(\frac{0.5-c}{a}\right)\frac{1}{b}$. In the case of thiophene and 3-methylthiophene as single-component ices, we did not destroy half of the organic molecules within the doses used in this study, and consequently the calculated radiolytic half-life is outside of the dose range. For this reason, we opt to denote the computed half-life dose as a lower limit, as is typical in such cases (e.g., Materese et al., 2020; Gerakines et al., 2022). Note that all uncertainties reported here were computed using standard error

296 propagation techniques (e.g., Taylor, 1982). Although we do not explicitly account for any
297 radiation-induced desorption or sputtering from our ice samples, these processes do not
298 substantially contribute to the apparent radiolytic destruction (see Brown et al., 1984 for
299 estimates of the sputtering of water ice by ~ 0.9 MeV protons).
300
301 **4. Discussion:**
302 **4.1 Radiolytic Destruction Rate Constants:**
303 As shown in Table 3 and Figures 7-9, the decomposition rate constant of thiophene and
304 thiophene derivative is larger in a water-ice matrix as compared to the single-component ices.
305 For example, the destruction rate constant of thiophene is a factor of 7.3 higher when irradiated
306 in a water-ice matrix as compared to a single-component ice at 20 K (0.08 vs. 0.011). This
307 behavior resembles that of other categories of organic molecules, including simple aromatics
308 (benzene; Ruiterkamp et al., 2005), amino acids (glycine; Gerakines et al., 2012; Gerakines and
309 Hudson, 2013), and nucleobases (thymine and uracil; Materese et al., 2020; Gerakines et al.,
310 2022). This enhanced decomposition is likely due to the additional reaction pathways provided
311 by the water molecules, ionized products, and neutral radicals. Studies of aqueous thiophene
312 have demonstrated the importance of H_2O radiolysis products, especially OH, H, and e^-, on the
313 production of thiophene radicals (Saunders et al., 1978; Saunders, 1978). This higher reactivity
314 in water-ice mixtures is also observed in our lower-temperature ice mixtures containing 2- and 3-
315 methylthiophene. At low temperatures, OH does not readily diffuse within an ice (Siegel et al.,
316 1961), and this may result in faster organic decomposition, possibly due to reactions between OH
317 radicals and neighboring thiophene-derivative molecules. Bierbach et al. (1992) demonstrated
318 that rate coefficients for gas-phase reactions between methylfuran and OH radicals were higher

than for reactions between furan and OH radicals. That study suggested that the substituted methyl group provided an inductive effect (i.e., additional electron density on the heterocyclic ring, attracting the strong electrophile OH; Marusawa et al., 2002) since methyl groups are less electron-withdrawing than a hydrogen atom. We note that H_2O_2 (a strong, low-temperature oxidant; Loeffler and Hudson, 2013) present in our low-temperature ices likely does not contribute to any thermally driven chemistry of thiophene or thiophene derivatives at these temperatures, since oxidation reactions between these species typically require catalysts at room temperature (Brown and Espenson, 1996). Materese et al. (2020) suggested that the water ice matrix structure (e.g., crystalline or amorphous) might affect the destruction of organics (thymine) at low temperatures, due to segregation of organics in more crystalline ices. While we cannot rule out a structural effect, the enhanced reactivity highlighted here occurs for only the methylated thiophenes, and our organics are effectively matrix isolated (100:1), which will suppress any rate enhancement due to matrix structure and resultant organic segregation (see Figure 7 from Materese et al., 2020).

In addition to the apparent matrix effects (i.e. single component or within a water-ice matrix), we find that the inclusion of a methyl functional group may subtly increase the destruction rate constant of the thiophene derivatives as compared to thiophene. This effect is most evident for the single-component ices at 125 K and in water-ice mixtures at 20 K. However, this is not the case for 3-methylthiophene as a single-component ice at low temperatures, and 2- and 3-methylthiophene diluted in water at high temperatures. This discrepancy for 3-methylthiophene at low temperatures is possibly due to the considerably smaller intrinsic band strength resulting in higher relative uncertainty in the fitted and computed parameters. For water-ice mixtures at high temperatures, we hypothesize that this difference

might be at least partially due to the increased diffusivity of OH radicals that results in fewer reactions between OH and neighboring methyl-substituted thiophenes.

Lastly, we note the appearance of a slight temperature dependence for our single-component ice samples, where the destruction rate constant for a single composition is higher at higher temperatures. This dependence could be due to a simple Arrhenius-like behavior (i.e., $k = e^{-E_a/RT}$ where E_a is the activation energy, R is the universal gas constant, and T is the temperature). An Arrhenius-like behavior would indicate that, at higher temperatures, more relevant to the Martian surface, the destruction rate constant would increase further. However, these results might also be partially explained by the amorphization of our crystalline ices. Our technique requires normalizing the band area of interest by the initial band area (i.e., A/A_0). The initial band (A_0) is due to entirely crystalline ice, and during irradiation, this band (A) might be only partially crystalline. Since the IR band strength of our amorphous samples is smaller than for the corresponding crystalline samples (determined during the warm-up experiments described in Section 3.1), we might be underestimating the amount of thiophene or thiophene derivative present. This amorphization effect is most evident in Figures 8 and 9 at 37 MGy, which suggests that we might be overestimating the amount of radiolytic destruction for our single-component ices at 125 K. Thus, these compounds might be even more stable on the surface of a planetary body than we report here, which is consistent with our discussion in the section below.

4.2 Implications for Astrobiology:

To best apply our laboratory data to the conditions of the Martian surface, we computed the radiation half-life for thiophene at 125 K as a single-component ice and for thiophene diluted in water ice at various depths (Table 4). We used the dose rates determined from data collected by

365 the Radiation Assessment Detector onboard the Mars Science Laboratory's Curiosity rover
366 (Hassler et al., 2014). As expected, the half-life for thiophene is significantly shorter when
367 diluted in a water-ice matrix as compared to a single-component ice. Based on previous work on
368 the radiolytic destruction of glycine in water and in carbon dioxide ice (Gerakines and Hudson,
369 2013, 2015), we expect that thiophene may also be more susceptible to radiation-driven
370 destruction in carbon dioxide than in water. This higher reactivity in carbon dioxide ice may be
371 important for the Martian surface, where diurnal cycling of CO_2 frost occurs even at low and
372 mid-latitudes (Piqueux et al., 2016). However, a detailed compositional study is outside the
373 scope of the present work and left for the future.
374 Half of the initial thiophene remains after approximately 130 and 530 million years (in water
375 ice and as a single-component ice, respectively) at the depths probed by the Curiosity rover drill
376 (~ 0.06 m; Millan et al., 2022). This stability increases substantially beyond one meter into the
377 surface. We emphasize that the data in Table 4 do not take into account all possible effects such
378 as surface heterogeneity in composition (i.e., matrix), regolith porosity, and temperature at a
379 given depth, which will all affect both the dose rates and the thiophene half-lives. Moreover,
380 macromolecules in which thiophene groups are embedded might provide additional radiation
381 resistance, which is not explored here. With these caveats in mind, we have demonstrated that
382 thiophene and mixtures of thiophene and water are degraded via radiolysis; however, much of
383 the thiophene at the Martian surface could remain for hundreds of millions of years and
384 significantly longer at depths greater than one meter. Furthermore, the surface exposure age of
385 the floor of Gale crater (where thiophene was detected) is estimated to be 80 Myr (Farley et al.,
386 2014), well within the radiation half-life of thiophene listed in Table 4. Consequently, thiophene,
387 produced from abiotic or biotic sulfur or organic molecules, could be stable on and near the

388 Martian surface for significant periods of time (~ 600 Myr) without the need of an active
389 replenishing source. The radiation stability of thiophene and, to a lesser extent, its derivatives
390 might explain their presence on the Martian surface.
391
392 **5. Conclusions**
393 We measured the radiation-driven destruction of thiophene, 2-methylthiophene, and 3-
394 methylthiophene at 20 K and 125 K as single-component ice**s** and when embedded in a water-ice
395 matrix (100:1). We quantified the radiolytic destruction with a pseudo first-order radiation
396 destruction rate constant and a radiolytic half-life. We found that the rate constant and half-life
397 depend strongly on temperature, where the rate constant increases with temperature in single-
398 component ices and decreases with increasing temperature in a water matrix. The methyl group
399 attached to the 2- and 3-methylthiophene might slightly affect the rate constant, decreasing the
400 compounds' radiolytic stability in some cases. From our radiolytic half-life for thiophene under
401 conditions most similar to the thiophene groups in Martian macromolecules and the established
402 surface radiation flux, we expect thiophene to be stable on the Martian surface for significantly
403 longer than the surface exposure age of the thiophene detection sample sites on the floor of Gale
404 crater (~ 600 Myr vs 80 Myr).
405
406 **Acknowledgements**
407 The material is based upon work supported by NASA under award number
408 80GSFC21M0002. This work is supported through GSFC Fundamental Laboratory Research
409 (FLaRe), and Goddard Center for Astrobiology. P.D.T. acknowledges Steve Brown and Eugene
410 Gerashchenko for operating and maintaining the Van de Graff Accelerator in the Radiation

411 Effects Facility at NASA GSFC, and Joseph Nuth for fruitful discussions. Data from this
412 publication are available in the following Zenodo repository: 10.5281/zenodo.13850669.
413

414 **References**

415 Acuña, M. H., Connerney, J. E. P., Wasilewski, P., Lin, R. P., Anderson, K. A., Carlson, C. W.,
416 McFadden, J., Curtis, D. W., Mitchell, D., Reme, H., Mazelle, C., Sauvaud, J. A.,
417 d'Uston, C., Cros, A., Medale, J. L., Bauer, S. J., Cloutier, P., Mayhew, M., Winterhalter,
418 D., and Ness, N. F. (1998). Magnetic field and plasma observations at Mars: initial results
419 of the Mars Global Surveyor mission. *Science*, **279** (5357), 1676-1680.
420 Bierbach, A., Barnes, I., and Becker, K. (1992). Rate coefficients for the gas-phase reactions of
421 hydroxyl radicals with furan, 2-methylfuran, 2-ethylfuran, and 2,5,-dimethylfuran at
422 300±2 K. *Atmospheric Environment Part A. General Topics*, **26** (5), 813-817.
423 Brown, K. N., and Espenson, J. H. (1996). Stepwise oxidation of thiophene and its derivatives by
424 hydrogen peroxide catalyzed by methyltrioxorhenium (VII). *Inorganic Chemistry*, **35**
425 (25), 7211-7216.
426 Brown, W. L., Augustyniak, W. M., Marcantonio, K. J., Simmons, E. H., Boring, J. W., Johnson,
427 R. E., and Reimann, C. T. (1984). Electronic sputtering of low temperature molecular
428 solids. *Nuclear Instruments and Methods in Physics Research B,* **1**, 307 – 314.
429 Cesaro, S. N., Dobos, S., and Stirling, A. (1999). FTIR spectra of thiophene in Ar and N_2
430 matrices. Co-condensation with Cu and CO. *Vibrational Spectroscopy,* **20** (1), 59-67.
431 Christensen, P. A., Hamnett, A., and Hillman, A. R. (1988). An in-situ infra-red study of poly
432 thiophene growth. *Journal of Electroanalytical Chemistry and Interfacial*
433 *Electrochemistry,* **242** (1-2), 47-62.

da Costa, C. A. P.; Souza-Corrêa, J. A., da Silveira, E. F. (2021). Infrared analysis of glycine dissociation by MeV ions and keV electrons. *Monthly Notices of the Royal Astronomical Society* **502**, 2105 – 2119.

Eigenbrode, J. L., Summons, R. E., Steele, A., Freissinet, C., Millan, M., Navarro-González, R., Sutter, B., McAdam, A. C., Franz, H. B., Glavin, D. P., Archer Jr., P. D., Mahaffy, P. R., Conrad, P. G., Hurowitz, J. A., Grotzinger, J. P., Gupta, S., Ming, D.W., Sumner, D. Y., Szopa, C., Malespin, C., Buch, A., and Coll, P. (2018). Organic matter preserved in 3-billion-year-old mudstones at Gale crater, Mars. *Science* **360** (6393), 1096-1101.

Espenson, J. H. (1981). *Chemical kinetics and reaction mechanisms*. McGraw-Hill Book Company.

Farley, K. A., Malespin, C., Mahaffy, P., Grotzinger, J. P., Vasconcelos, P. M., Milliken, R. E., Malin, M., Edgett, K. S., Pavlov, A. A., Hurowitz, J. A., Grant, J. A., Miller, H. B., Arvidson, R., Beegle, L., Calef, F., Conrad, P. G., Dietrich, W. E., Eigenbrode, J., Gellert, R., Gupta, S., Hamilton, V., Hassler, D. M., Lewis, K. W., McLennan, S. M., Ming, D., Navarro-González, R., Schwenzer, S. P., Steele, A., Stolper, E. M., Sumner, D. Y., Vaniman, D., Vasavada, A., Williford, K., Wimmer-Schweingruber, R. F., and the MSL Science Team (2014). In situ radiometric and exposure age dating of the Martian surface. *Science,* **343** (6169), 1247166.

Freissinet, C., Glavin, D. P., Mahaffy, P. R., Miller, K. E., Eigenbrode, J. L., Summons, R. E., Brunner, A. E., Buch, A., Szopa, C., Archer Jr., P. D., Franz, H. B., Atreya, S. K., Brinckerhoff, W. B., Cabane, M., Coll, P., Conrad, P. G., Des Marais, D. J., Dworkin, J. P., Fairén, A. G., François, P., Grotzinger, J. P., Kashyap, S., ten Kate, I. L., Leshin, L. A., Malespin, C. A., Martin, M. G., Martin-Torres, F. J., McAdam, A. C., Ming, D. W.,

Navarro-González, R., Pavlov, A. A., Prats, B. D., Squyres, S. W., Steele, A., Stern, J. C., Sumner, D. Y., Sutter, B., Zorzano, M.-P., and the MSL Science Team (2015). Organic molecules in the Sheepbed mudstone, Gale crater, Mars. *Journal of Geophysical Research: Planets,* **120** (3), 495–514.

Gerakines, P. A., and Hudson, R. L. (2013). Glycine's radiolytic destruction in ices: first *in situ* laboratory measurements for Mars. *Astrobiology*, **13** (7), 647-655.

Gerakines, P. A., and Hudson, R. L. (2015). The radiation stability of glycine in solid CO_2-*in situ* laboratory measurements with applications to Mars. *Icarus*, **252**, 466-472.

Gerakines, P. A., Hudson, R. L., Moore, M. H., and Bell, J.-L. (2012). *In situ* measurements of the radiation stability of amino acids at 15-140 K. *Icarus*, **220** (2), 647-659.

Gerakines, P. A., Qasim, D., Frail, S., and Hudson, R. L. (2022). Radiolytic destruction of uracil in interstellar and solar system ices. *Astrobiology*, **22** (3), 233-241.

Guzman, M., McKay, C. P., Quinn, R. C., Szopa, C., Davila, A. F., Navarro-González, R., and Freissinet, C. (2018). Identification of chlorobenzene in the Viking gas chromatograph-mass spectrometer data sets: reanalysis of Viking mission data consistent with aromatic organic compounds on Mars. *Journal of Geophysical Research: Planets*, **123** (7), 1674-1683.

Hagen, W., Tielens, A. G. G. M., and Greenberg, J. M. (1981). The infrared spectra of amorphous solid water and ice i_c between 10 and 140 K. *Chemical Physics*, **56** (3), 367-379.

Hardin, A. H., and Harvey, K. B. (1973). Temperature dependences of the ice i hydrogen bond spectral shifts – i: The vitreous to cubic ice i phase transformation. *Spectrochimica Acta Part A: Molecular Spectroscopy,* **29** (6), 1139-1151.

Hassler, D. M., Zeitlin, C., Wimmer-Schweingruber, R. F., Ehresmann, B., Rafkin, S., Eigenbrode, J. L., Brinza, D. E., Weigle, G., Böttcher, S., Böhm, E., Burmeister, S., Guo, J., Köhler, J., Martin, C., Reitz, G., Cucinotta, F. A., Kim, M.-H., Grinspoon, D., Bullock, M. A., Posner, A., Gómez-Elvira, J., Vasavada, A., Grotzinger, J. P., and Team, M. S. (2014). Mars' surface radiation environment measured with the Mars Science Laboratory's Curiosity rover. *Science*, **343** (6169), 1244797.

Heavens, O. S. (2011). *Optical Properties of Thin Solid Films*. New York: Dover.

Heinz, J., and Schulze-Makuch, D. (2020). Thiophenes on Mars: biotic or abiotic origin? *Astrobiology*, **20** (4), 552-561.

Hiraoka, H., Srinivasan, R. (1968). Photoisomerization of 2-alkylfurans to 3-alkylfurans. *Journal of the American Chemical Society,* **90** (10), 2720-2721.

Hornig, D. F., White, H. F., and Reding, F. P. (1958). The infrared spectra of crystalline H_2O, D_2O and HDO. *Spectrochimica Acta*, **12** (4), 338-349.

Hudson, R. L., and Ferrante, R. F. (2020). Quantifying acetaldehyde in astronomical ices and laboratory analogues: IR spectra, intensities, 13C shifts, and radiation chemistry. *Monthly Notices of the Royal Astronomical Society,* **492** (1), 283-293.

Hudson, R. L., and Yarnall, Y. Y. (2022). Infrared spectra and optical constants of astronomical ices: IV. Benzene and pyridine. *Icarus*, **377**, 114899.

Kellogg, R. M., Dik, J. K., van Driel, H., and Wynberg, H. (1970). Photochemistry of thiophenes. IX. Rearrangements of alkylthiophenes and the dithienyls. *The Journal of Organic Chemistry,* **35** (8), 2737-2741.

Kim, Y. S., Inui, H., and McMahon, R. J. (2006). Ring opening of 2,5-didehydrothiophene: matrix photochemistry of C_4H_2S isomers. *The Journal of Organic Chemistry,* **71** (26), 9602-9608.

Li, H., Lang, J., Foley, C. D., Zádor, J., and Suits, A. G. (2023). Sulfur (^3P) reaction with conjugated dienes gives cyclization to thiophenes under single collision conditions. *The Journal of Physical Chemistry Letters*, **14** (34), 7611-7617.

Loeffler, M. J., and Hudson, R. L. (2013). Low-temperature thermal reactions between SO_2 and H_2O_2 and their relevance to the jovian icy satellites. *Icarus*, **224** (1), 257-259.

Loeffler, M. J., and Hudson, R. L. (2018). Coloring Jupiter's clouds: radiolysis of ammonium hydrosulfide (NH_4SH). *Icarus*, **302**, 418-425.

Marusawa, H., Ichikawa, K., Narita, N., Murakami, H., Ito, K., and Tezuka, T. (2002). Hydroxyl radical as a strong electrophilic species. *Bioorganic and Medicinal Chemistry,* **10** (7), 2283-2290.

Materese, C. K. (2022). Radiation-induced D-to-H exchange in ices containing ethane or benzene: reactions and rate constants. *The Astrophysical Journal,* **941** (1), 94.

Materese, C. K., Gerakines, P. A., and Hudson, R. L. (2020). The radiation stability of thymine in solid H_2O. *Astrobiology,* **20** (8), 956-963.

Mejía, C., da Costa, C. A. P., Iza, P., da Silveira, E. F. (2022). Irradiation of phenylalanine at 300 K by MeV ions. *Astrobiology,* **22** (4), 439 – 451.

Mejía, C., Vignoli Muniz, G. S., Bender, M., Severin, D., Trautmann, C., Augé, B., Agnihotri, A. N., Boduch, P., Domaracka, A., Rothard, H. (2023). Swift heavy ion irradiation of thymine at cryogenic temperature. *Nuclear Instruments and Methods in Physics Research, B*, **534**, 11 – 15.

Migliorini, M. G., Salvi, P. R., and Sbrana, G. (1974). New spectroscopic evidence of the four solid modifications of thiophene. *Chemical Physics Letters,* **28** (4), 565-568.

Millan, M., Williams, A. J., McAdam, A. C., Eigenbrode, J. L., Steele, A., Freissinet, C., Glavin, D. P., Szopa, C., Buch, A., Summons, R. E., Lewis, J. M. T., Wong, G. M., House, C. H., Sutter, B., McIntosh, O., Bryk, A. B., Franz, H. B., Pozarycki, C., Stern, J. C., Navarro-González, R., Archer, D. P., Fox, V., Bennett, K., Teinturier, S., Malespin, C., Johnson, S. S., and Mahaffy, P. R. (2022). Sedimentary organics in Glen Torridon, Gale crater, Mars: results from the SAM instrument suite and supporting laboratory analyses. *Journal of Geophysical Research: Planets*, **127** (11), e2021JE007107.

Miyazaki, Y., Nakano, M., Krivchikov, A. I., Koroyuk, O. A., Gebbia, J. F., Cazorla, C., and Tamarit, J. L. (2021). Low-temperature heat capacity anomalies in ordered and disordered phases of normal and deuterated thiophene. *The Journal of Physical Chemistry Letters*, **12** (8), 2112–2117.

Moll, N. G., Clutter, D. R., and Thompson, W. E. (1966). Carbon trioxide: its production, infrared spectrum, and structure studied in a matrix of solid CO_2. *The Journal of Chemical Physics*, **45**, 4469–4481.

Moore, M. H. and Hudson, R. L. (1998). Infrared study of ion-irradiated water-ice mixtures with hydrocarbons relevant to comets. *Icarus*, **135** (2), 518–527.

Moore, M. H., Khanna, R., and Donn, B. (1991). Studies of proton irradiated H_2O+CO_2 and H_2O+CO ices and analysis of synthesized molecules. *Journal of Geophysical Research: Planets*, **96** (E2), 17541–17545.

545 Narten, A. H., Venkatesh, C. G., and Rice, S. A. (1976). Diffraction pattern and structure of
546 amorphous solid water at 10 and 77 K. *The Journal of Chemical Physics*, **64** (3), 1106–
547 1121.
548 Palumbo, M. E., Baratta, G. A., Brucato, J. R., Castorina, A. C., Satorre, M. A., and Strazzulla,
549 G. (1998). Profile of the CO_2 bands produced after ion irradiation of ice mixtures.
550 *Astronomy and Astrophysics*, **334**, 247–252.
551 Pennington, R. E., Finke, H. L., Hubbard, W. N., Messerly, J. F., Frow, F. R., Hossenlopp, I. A.,
552 and Waddington, G. (1956). The chemical thermodynamic properties of 2-
553 methylthiophene. *Journal of the American Chemical Society*, **78** (10), 2055–2060.
554 Pimblott, S. M., and LaVerne, J. A. (2007). Production of low-energy electrons by ionizing
555 radiation. *Radiation Physics and Chemistry*, **76** (8-9), 1244-1247.
556 Piqueux, S., Kleinböhl, A., Hayne, P. O., Heavens, N. G., Kass, D. M., McCleese, D. J.,
557 Schofield, J. T., and Shirley, J. H. (2016). Discovery of a widespread low-latitude diurnal
558 CO_2 frost cycle on Mars. *Journal of Geophysical Research: Planets*, **121** (7), 1174–1189.
559 Qasim, D., Hudson, R. L., and Materese, C. K. (2022). Radiation-induced D/H exchange rate
560 constants in aliphatics embedded in water ice. *The Astrophysical Journal*, **929** (2), 176.
561 Qi, F., Sorkhabi, O., Rizvi, A. H., and Suits, A. G. (1999). 193 nm photodissociation of
562 thiophene probed using synchrotron radiation. *The Journal of Physical Chemistry A*, **103**
563 (42), 8351–8358.
564 Quigley, W. W. C., Yamamoto, H. D., Aegerter, P. A., Simpson, G. J., and Bussell, M. E.
565 (1996). Infrared spectroscopy and temperature-programmed desorption study of adsorbed
566 thiophene on γ-Al_2O_3. *Langmuir*, **12** (6), 1500–1510.

Rasch, B. and Vielstich, W. (1994). Polythiophenes via thiophene, bithiophene and terthiophene in propylene carbonate: an electrochemical and in-situ FTIR study. *Journal of Electroanalytical Chemistry*, **370** (1-2), 109–117.

Rico, M., Orza, J. M., and Morcillo, J. (1965). Fundamental vibrations of thiophene and its deuterated derivatives. *Spectrochimica Acta*, **21** (4), 689–719.

Ruiterkamp, R., Peeters, Z., Moore, M. H., Hudson, R. L., and Ehrenfreund, P. (2005). A quantitative study of proton irradiation and UV photolysis of benzene in interstellar environments. *Astronomy and Astrophysics*, **440** (1), 391–402.

Saunders, B. B. (1978). Reactions of thiophene with radiolytically produced radicals. 2. The solvated electron and the hydrogen atom. *The Journal of Physical Chemistry*, **82** (2), 151–154.

Saunders, B. B., Kaufman, P. C., and Matheson, M. S. (1978). Reactions of thiophene with radiolytically produced radicals. 1. The hydroxyl radical. *The Journal of Physical Chemistry*, **82** (2), 142–150.

Siegel, S., Flournoy, J. M., and Baum, L. H. (1961). Irradiation yields of radicals in gamma irradiated ice at 4.2 and 77 K. *The Journal of Chemical Physics*, **34** (5), 1782–1788.

Strazzulla, G. and Baratta, G. A. (1991). Laboratory study of the IR spectrum of ion-irradiated frozen benzene. *Astronomy and Astrophysics*, **241** (1), 310–316.

Taylor, J. R. (1982). An introduction to error analysis: the study of uncertainties in physical measurements. Springer, 2nd edition.

Tolbert, B. M. and Lemmon, R. M. (1955). Radiation decomposition of pure organic compounds. *Radiation Research*, **3** (1), 52–67.

589 Vasavada, A. R. (2022). Mission overview and scientific contributions from the Mars Science
590 Laboratory Curiosity rover after eight years of surface operations. *Space Science*
591 *Reviews*, **218** (3), 14.
592 Vasavada, A. R., Piqueux, S., Lewis, K. W., Lemmon, M. T., and Smith, M. D. (2017).
593 Thermophysical properties along Curiosity's traverse in Gale crater, Mars, derived from
594 the REMS ground temperature sensor. *Icarus*, **284**, 372–386.
595 Vignoli Muniz, G. S., Agnihotri, A. N., Augé, B., Mejía, C., Martinez, R., Rothard, H.,
596 Domaracka, A., and Boduch, P. (2022). Radiolysis of cytosine at cryogenic temperatures
597 by swift heavy ion bombardments. *ACS Journal of Earth and Space Chemistry*, **6**, 2149 –
598 2157.
599 Weast, R. C., Sudy, S., and Hodman, C. (1984). Handbook of Chemistry and Physics. Boca
600 Raton, FL: CRC Press.
601 Wray, J. J. (2013). Gale crater: the Mars Science Laboratory/Curiosity rover landing site.
602 *International Journal of Astrobiology*, **12** (1), 25–38.
603 Wynberg, H. and Bantjes, A. (1959). Pyrolysis of thiophene. *The Journal of Organic Chemistry*,
604 **24** (10), 1421–1423.
605 Yarnall, Y. Y. and Hudson, R. L. (2022a). Crystalline ices–densities and comparisons for
606 planetary and interstellar applications. *Icarus*, **373**, 114799.
607 Yarnall, Y. Y. and Hudson, R. L. (2022b). A new method for measuring infrared band strengths
608 in H_2O ices: first results for OCS, H_2S, and SO_2. *The Astrophysical Journal Letters*, **931**
609 (1), L4.

Ziegler, J. F., Ziegler, M. D., and Biersack, J. P. (2010). SRIM–The stopping and range of ions in matter (2010). *Nuclear Instruments and Methods in Physics Research Section B:Beam Interactions with Materials and Atoms*, **268** (11-12), 1818–1823.

Table 1: Density and index of refraction at 670 nm, and the calculated total stopping power and projected range of 0.9 MeV p^+ in thiophene, 2-methylthiophene, 3-methylthiophene, and when diluted in water. [a] The density and index of refraction were determined at 18 K. [b] H_2O HPLC Grade, Fisher Chemical. [c] Narten et al. (1976); compact amorphous H_2O ice, 77 K. [d] Weast et al. (1984). [e] Values for 100:1 mixtures of water and thiophene and thiophene derivatives, respectively.

Compound	Density [a] /g cm^{-3}	Index of Refraction [a] (n_{vis})	Total Stopping Power /10^8 eV cm^2 g^{-1}	Proton Range /μm
Thiophene (≥ 99%, Sigma Aldrich)	0.894	1.424	2.45	**26**
2-methylthiophene (98%, Sigma Aldrich)	0.809	1.389	2.54	**27.6**
3-methylthiophene (98%, Sigma Aldrich)	0.813	1.387	2.54	**27.5**
Diluted in Water [b] (100:1)	0.94 [c]	1.31 [d]	2.67; 2.68 [e]	**22.7**

Table 2: Curve fit parameters for the radiolytic destruction of thiophene and thiophene derivatives. [a] All mixtures with water have a relative abundance of 100:1 water:organic.

		Curve fit parameters for $ae^{-bD} + c$		
Composition [a]	T /K	a	b	c
Thiophene	20	0.59 ± 0.02	0.019 ± 0.001	0.41 ± 0.02
Thiophene	125	0.71 ± 0.02	0.024 ± 0.002	0.29 ± 0.02
2-methylthiophene	20	0.73 ± 0.02	0.019 ± 0.001	0.28 ± 0.02
2-methylthiophene	125	0.93 ± 0.02	0.020 ± 0.004	0.10 ± 0.09
3-methylthiophene	20	0.9 ± 0.2	0.009 ± 0.003	0.1 ± 0.1
3-methylthiophene	125	0.79 ± 0.05	0.024 ± 0.003	0.24 ± 0.06
H_2O + thiophene	20	0.90 ± 0.05	0.09 ± 0.01	0.12 ± 0.05
H_2O + thiophene	125	0.62 ± 0.03	0.13 ± 0.02	0.37 ± 0.03
H_2O + 2-methylthiophene	20	0.86 ± 0.02	0.16 ± 0.01	0.14 ± 0.02
H_2O + 2-methylthiophene	125	0.72 ± 0.06	0.064 ± 0.009	0.30 ± 0.06
H_2O + 3-methylthiophene	20	0.9 ± 0.1	0.09 ± 0.02	0.1 ± 0.1
H_2O + 3-methylthiophene	125	0.69 ± 0.07	0.09 ± 0.02	0.29 ± 0.07

627

628 *Table 3: Rate constants and radiolytic half-lifes for thiophene and thiophene derivatives. [a]All mixtures with water have a*
629 *relative abundance of 100:1 water :organic. [b] k_1 was calculated using fitted parameters a and b. [c] Note that for two*
630 *samples (low-temperature thiophene and 3-methylthiophene) only a lower limit could be established for the radiation*
631 *half-life (see text).*

Composition [a]	T /K	k_1 /MGy^{-1} [b]	Half-Life /MGy [c]
Thiophene	20	0.011 ± 0.001	> 80
Thiophene	125	0.017 ± 0.001	51 ± 4
2-methylthiophene	20	0.014 ± 0.001	63 ± 5
2-methylthiophene	125	0.019 ± 0.004	42 ± 12
3-methylthiophene	20	0.008 ± 0.003	> 80
3-methylthiophene	125	0.019 ± 0.002	46 ± 16
H_2O + thiophene	20	0.08 ± 0.01	10 ± 2
H_2O + thiophene	125	0.08 ± 0.01	12 ± 2
H_2O + 2-methylthiophene	20	0.14 ± 0.01	5.4 ± 0.4
H_2O + 2-methylthiophene	125	0.046 ± 0.008	20 ± 5
H_2O + 3-methylthiophene	20	0.08 ± 0.03	9 ± 3
H_2O + 3-methylthiophene	125	0.06 ± 0.01	13 ± 4

632

633

634 *Table 4: Dose rates at and under the Martian surface, and calculated thiophene (T), 2-methylthiophene (2MT), and 3-*
635 *methylthiophene (3MT) half-lifes ($t_{1/2}$) at 125 K. [a] Hassler et al. (2014).*

Depth /m	Dose Rate /mGy yr^{-1} [a]	Thiophene $t_{1/2}$ /10^9 yr		2MT $t_{1/2}$ /10^9 yr		3MT $t_{1/2}$ /10^9 yr	
		T	in H_2O ice	2MT	in H_2O ice	3MT	in H_2O ice
0	76	0.67	0.16	0.55	0.26	0.61	0.17
0.1	96	0.53	0.13	0.44	0.21	0.48	0.14
1.0	36	1.4	0.33	1.2	0.56	1.3	0.36
2.0	8.7	5.9	1.4	4.8	2.3	5.3	1.5
3.0	1.8	28	6.7	23	11	26	7.2

636

637

638

639

640 Figures and Captions

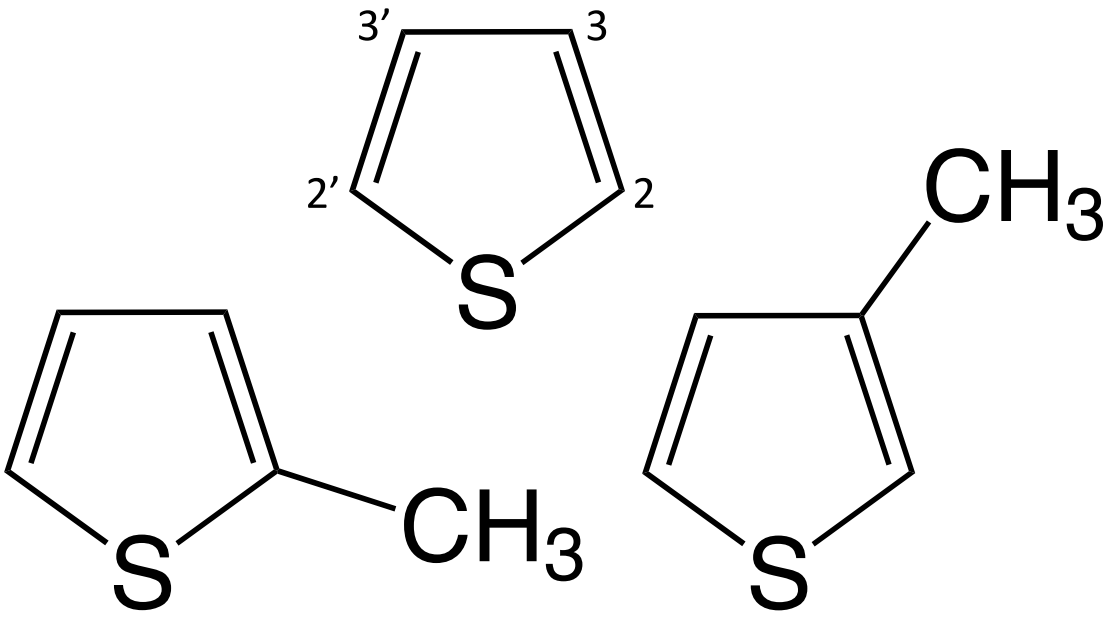

641

642 Figure 1: Molecular structures of thiophene (top), 2-methylthiophene (left), and 3-

643 methylthiophene (right).

644

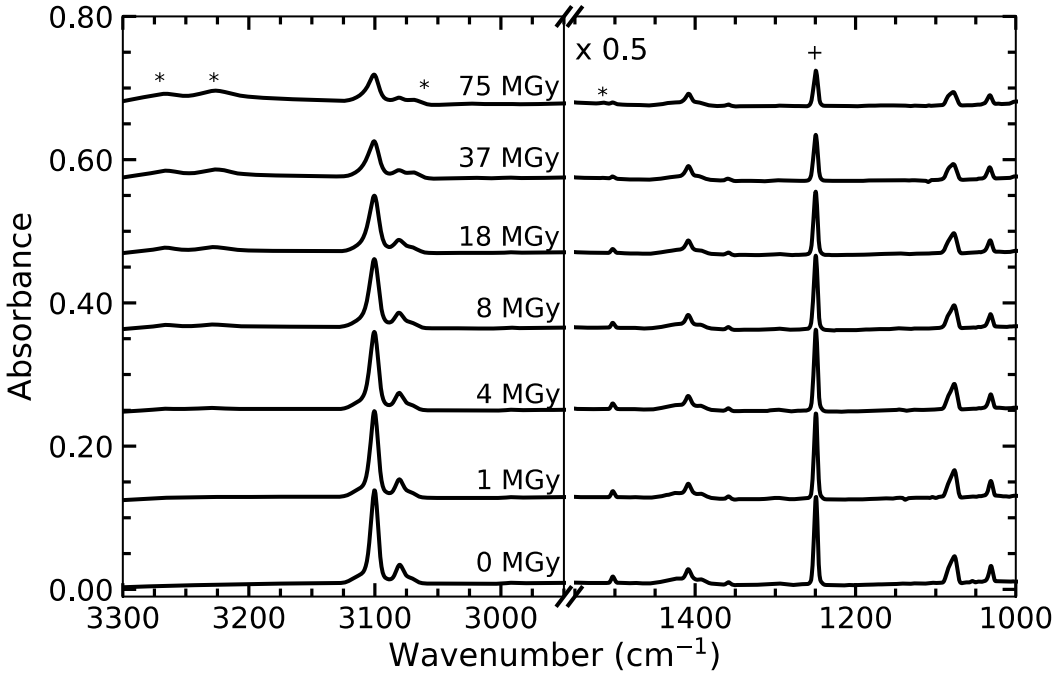

645

Figure 2: Infrared spectra of thiophene irradiated at 125 K. From bottom to top, spectra correspond to radiation doses of 0, 1, 4, 8, 18, 37, 75 MGy. The plus sign and asterisk correspond to the fundamental thiophene band of interest and a radiolytic product, respectively. Spectra are vertically offset for clarity, and the lower wavenumber range spectra (right panel) have been scaled by 0.5 for clarity.

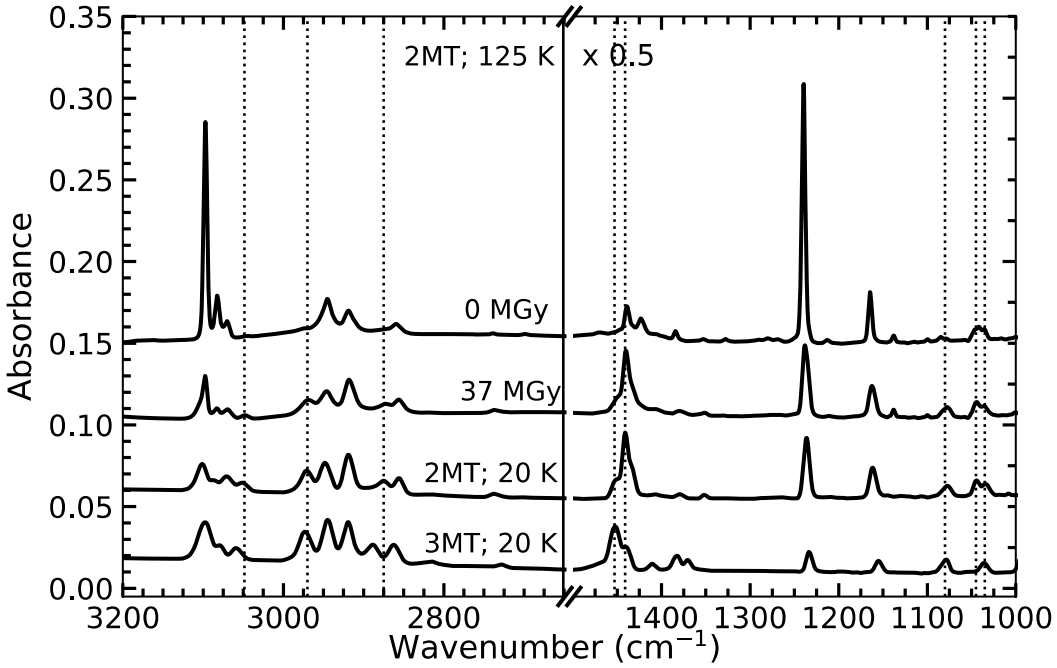

Figure 3: Infrared spectra of 2-methylthiophene (2MT) irradiated at 125 K, and unirradiated 2MT and 3-methylthiophene (3MT) for comparison. From the top to the bottom, spectra correspond to 2MT grown at 125 K, 2MT grown at 125 K and irradiated to a dose of 37 MGy, 2MT grown at 20 K, and 3MT grown at 20 K. Spectra are vertically offset for clarity. Vertical dotted lines indicate spectral features that increase with dose and correspond to reference spectral features.

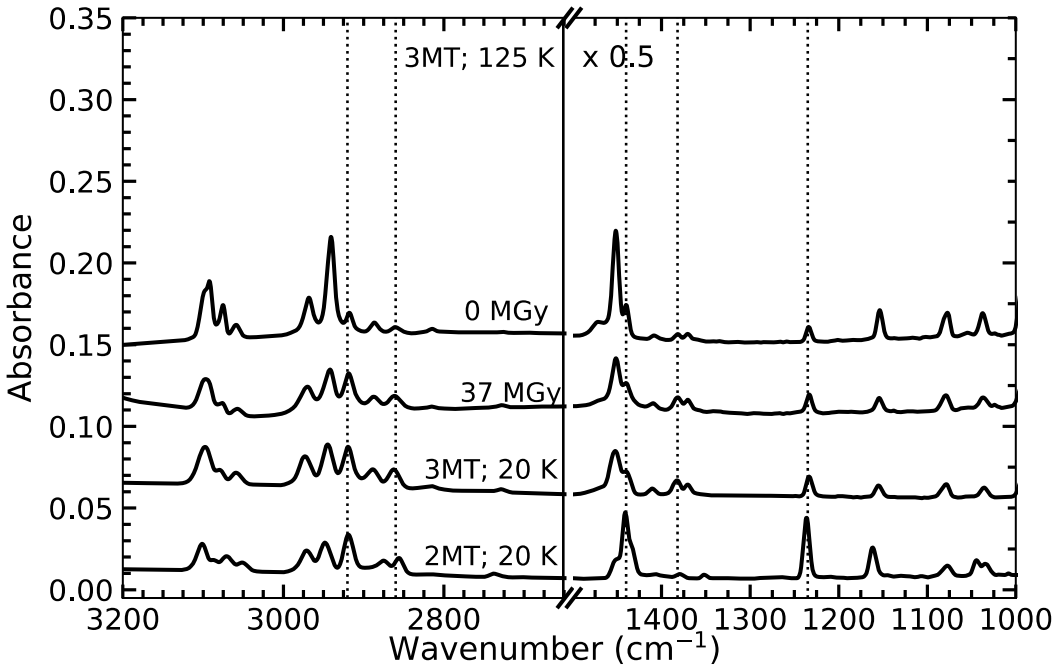

Figure 4: Infrared spectra of 3-methylthiophene (3MT) irradiated at 125 K, and unirradiated 3MT and 2-methylthiophene (2MT) for comparison. From the top to the bottom, spectra correspond to 3MT grown at 125 K, 3MT grown at 125 K and irradiated to a dose of 37 MGy, 3MT grown at 20 K, and 2MT grown at 20 K. Spectra are vertically offset for clarity. Vertical dotted lines indicate spectral features that increase with dose and correspond to reference spectral features.

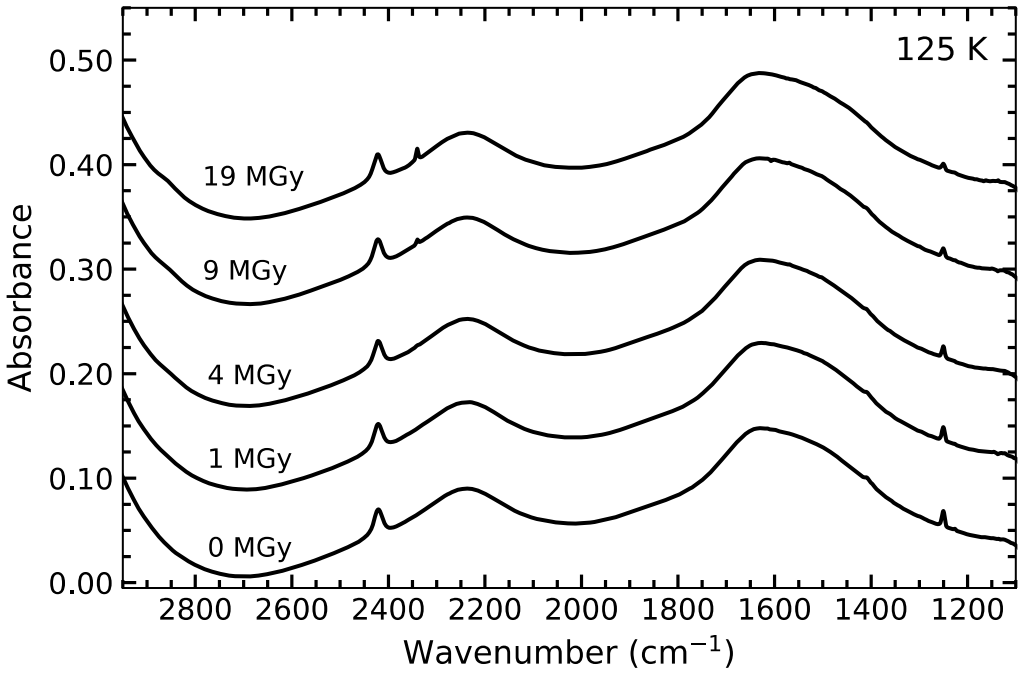

668

669 Figure 5: Infrared spectra of a mixture of water ice and thiophene (100:1) irradiated at 125 K.

670 From bottom to top, spectra correspond to radiation doses of 0, 1, 4, 9, 19 MGy. Spectra are

671 vertically offset for clarity.

672

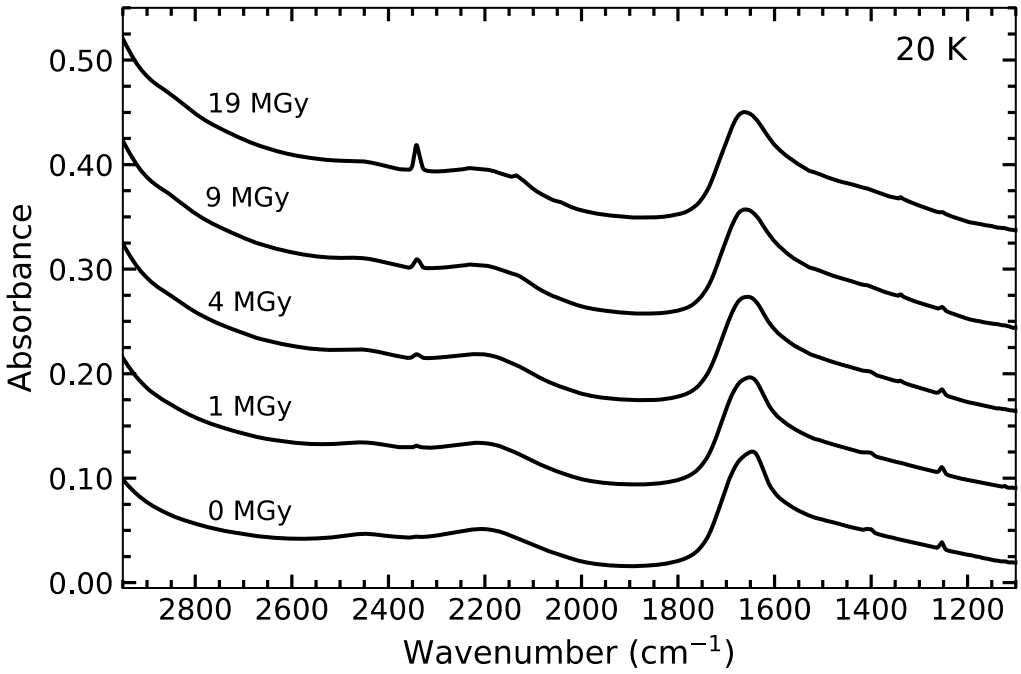

673

674 Figure 6: Infrared spectra of a mixture of water ice and thiophene (100:1) irradiated at 20 K.

675 From bottom to top, spectra correspond to radiation doses of 0, 1, 4, 9, 19 MGy. Spectra are

676 vertically offset for clarity.

677

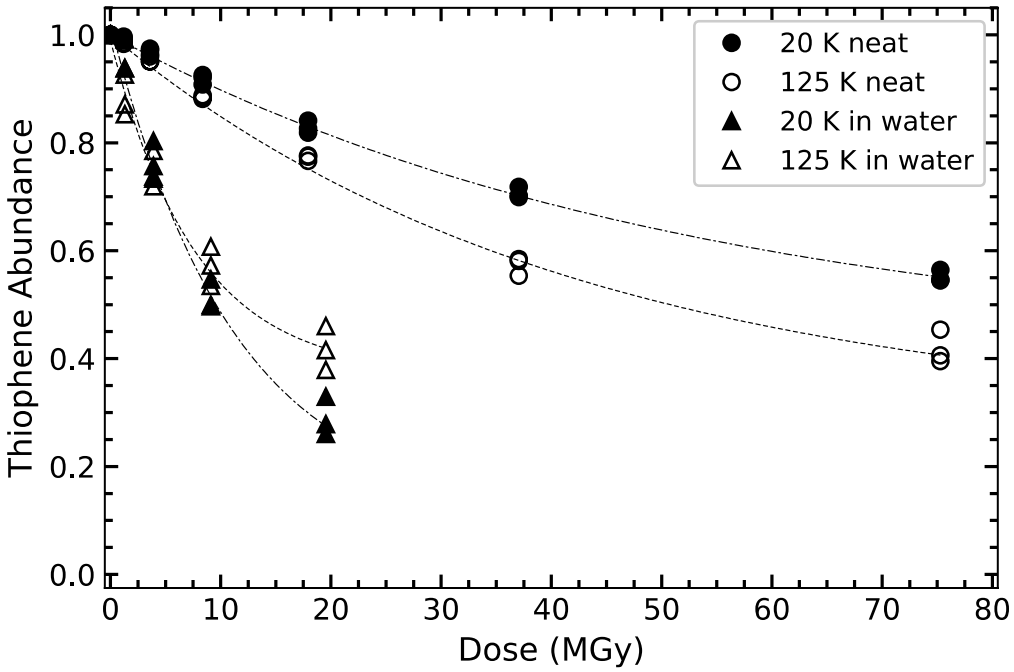

678

679 Figure 7: Normalized thiophene abundance (A/A_0) as a function of radiation dose for neat ices

680 (circles) and water-ice mixtures (triangles) at 20 K (solid symbols) and 125 K (open symbols)

681 with the corresponding best-fit decay curve for 20 K (dashed-dotted) and 125 K (dashed) data

682 sets.

683

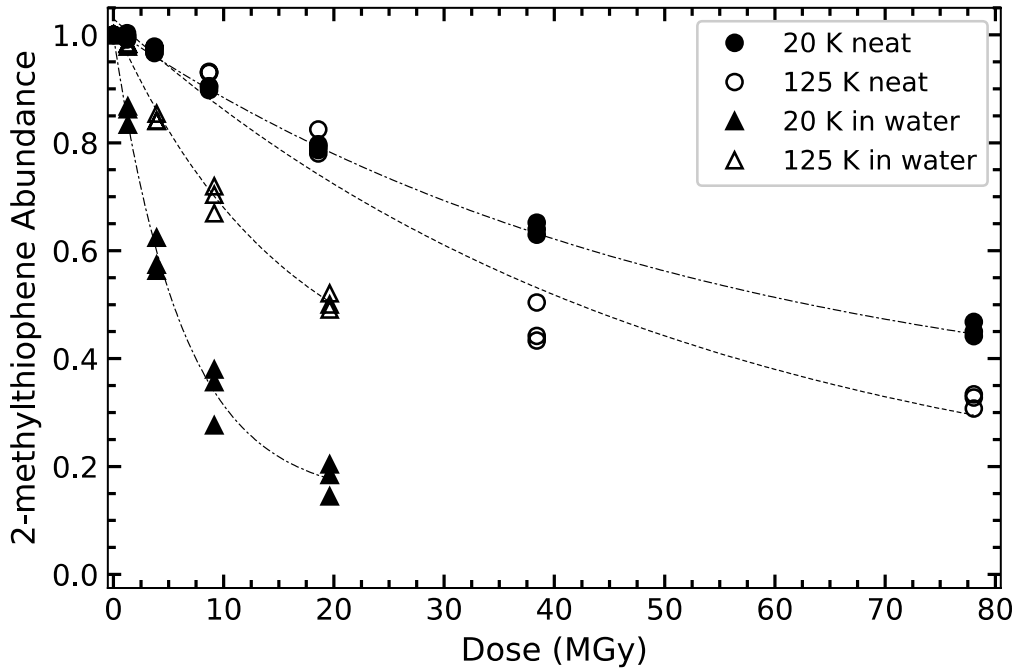

Figure 8: Normalized 2-methylthiophene abundance (A/A_0) as a function of radiation dose for neat ices (circles) and water-ice mixtures (triangles) at 20 K (solid symbols) and 125 K (open symbols) with the corresponding best-fit decay curve for 20 K (dash-dotted) and 125 K (dashed) data sets.

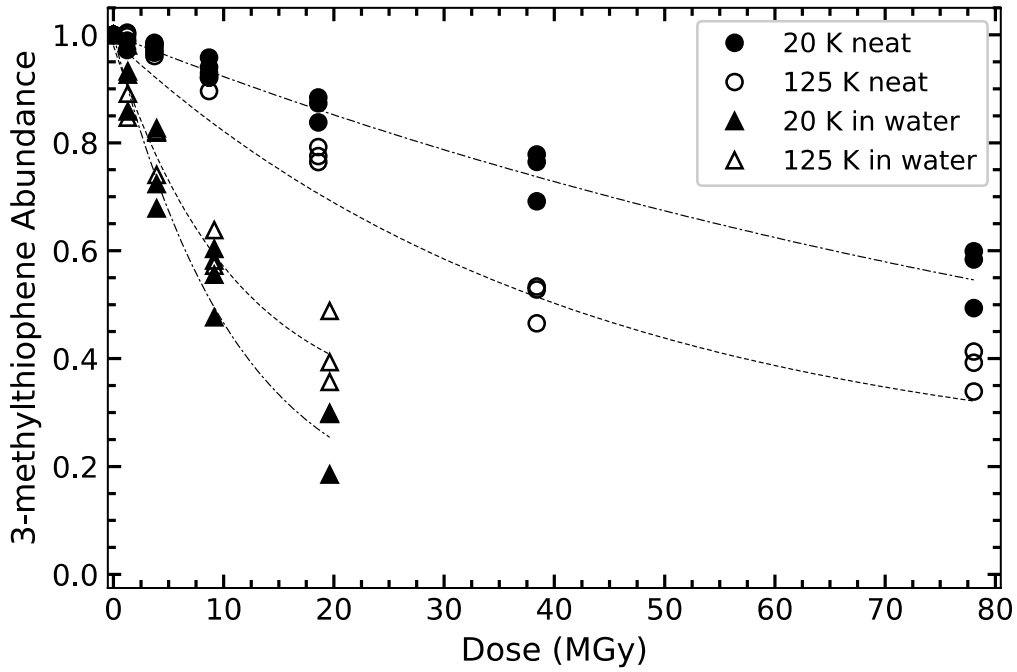

690

691 Figure 9: Normalized 3-methylthiophene abundance (A/A_0) as a function of radiation dose for
692 neat ices (circles) and water-ice mixtures (triangles) at 20 K (solid symbols) and 125 K (open
693 symbols) with the corresponding best-fit decay curve for the 20 K (dashed-dotted) and 125 K
694 (dashed) data sets.

695

696

697